Winter 1-8-2021

Single-Beam Inscription of Plasmon-Induced Surface Gratings

Denis AB Therien
The University of Western Ontario

Nina M. Culum
The University of Western Ontario

Danielle M. McRae
The University of Western Ontario

Leila Mazaheri
The University of Western Ontario, lmazaher@uwo.ca

Francois Lagugne-Labarthet
University of Western Ontario, flagugne@uwo.ca

Single-Beam Inscription of Plasmon-Induced Surface Gratings

Denis A. B. Therien, Nina M. Ćulum, Danielle M. McRae, Leila Mazaheri and François Lagugné-Labarthet**

University of Western Ontario (Western University), Department of Chemistry, 1151 Richmond St., London, Ontario, Canada, N6A 5B7

Abstract

The formation of gratings on gold nanoprisms arrays by plasmon-mediated reduction of a diazonium salt is investigated. Nanosphere lithography (NSL) is used to produce large surfaces of gold nanoprisms that are effective at reducing diazonium salts by producing hot electrons through excitation of localized surface plasmon resonances (LSPRs). Using single beam irradiation, we report here on the formation of periodic structures formed from the diazonium salts and that follow the NSL structures. On plasmonically active nanoprism substrates, the electric field enhancement promotes chemical reduction and hence modifies the grafting direction and grating properties of the ripples. The nanoprisms act as a plasmon guide which widens the pitch of the self-organized gratings and can even alter it from straight lines into a crisscross pattern.

Keywords: Plasmon-mediated grafting, self-organized gratings, plasmonic, nanosphere lithography, surface chemistry, diazonium salt reduction

*Corresponding Author. E-mail addresses: lmazaher@uwo.ca (L. Mazaheri) and flagugne@uwo.ca (F. Lagugné-Labarthet).

1. Introduction

Highly periodic surface gratings can develop upon single beam illumination on solids and liquids using either continuous-wave (CW) or pulsed lasers, provided that the illumination has a sufficient energy density [1]. Self-organized regular patterns emerge from interaction between an input optical field of the single beam and an initial variation of the physical or electromagnetic properties of the illuminated surface [2-3].These self-organized gratings produced under pulsed illumination are usually referred to as laser-induced periodic surface structures (LIPSS) in literature, where the irreversible ripples form lines parallel to the polarization direction [3-5]. The formation process and the subsequent grating properties can differ noticeably depending on the experimental opto-geometric conditions such as laser intensity, polarization state, angle of incidence, wavelength, material roughness and index of refraction of the sample.

The self-organization mechanism is explained considering the formation of a spontaneous interference pattern and its coupling with the substrate that yields the structure formation [1, 6]. Self-organized structures can appear on surfaces which support plasmons modes, polaritons, or surface-standing waves [7-10], as well as bare dielectric surfaces [11-12]. Specifically, the formation of self-organized interference patterns is correlated with the coupling between the incident beam and the scattered beam onto the surface of the sample. This self-organization mechanism is analogous to Wood's anomalies in metallic diffraction gratings whereby coupling of one of the primary diffraction orders with the sample is effective at the grazing angle [1]. The sample surface can have initial variation of any optical physical properties. Examples of such surface irregularities include surface roughness, defect density, or gradient of refraction index.

Surface irregularities can be considered as a spatial frequency which diffracts the incident beam into different directions following the Rayleigh diffraction law [1, 13]. The incident beam is perturbated from the surface irregularities and scattered into different directions depending on the incoming wavelengths and the incident angle. One range of surface irregularities with a specific spatial frequency can scatter the beam into the surface of the sample. The interference pattern formed by the input beam and the scattered contribution at the grazing angle will impinge on the sample surface and interact with the material. Light-matter interaction further enhances the surface irregularities in a feedback loop fashion. This spatial frequency of the surface irregularities yields interference patterns that couple with the material and grow in size until it reaches an optimal condition, in which other initial irregularities are washed out and periodic structures are formed [12]. The induction of the periodic structures by self-organized light can have distinct origins such as thermal (e.g., melting, phase transitions, recrystallization, and vaporization), saturable absorption and mass movement, plasma formation, surface chemical changes, refractive index changes, photodegradation, and photoetching[1, 6, 12, 14].

In this paper, we report self-organization of LIPSS investigated on two types of surfaces: a bare glass and a plasmonic substrate. These substrates were immersed in a solution containing diazonium salts and irradiated with a single laser beam. Photochemical and plasmon-mediated reactions appear to direct the structure formation in specific fashions. The possible mechanisms for the reduction of the diazonium salts with metallic nanostructures has been reported, highlighting the role of the shape and the optical properties of the structures. In particular, it was shown that diazonium salts polymerize in polyaryl films predominantly through a radical process in the area where the induction of hot electrons is maximized [15]. In this work, we investigated the formation of a ripple structure at the interface of glass and diazonium salt-containing solution.

We further modified the substrate by introducing plasmonically active gold nanoprisms produced by nanosphere lithography (NSL). In this paper, we highlight the difference in the formation of these ripple structures on bare glass and plasmonic substrates.

2. Experimental

Nanosphere Lithography (NSL): Nanosphere lithography was performed on glass coverslips (22 mm × 22 mm × 0.16 mm). A colloidal solution of 1 μm polystyrene spheres (Thermofisher Scientific) was prepared. A rubber O-ring was placed on the surface of the coverslips, and the polystyrene bead solution was drop-casted into the center and air dried for 24 hours. Once dried, the substrates were coated with 3 nm of titanium (adhesion layer) and 30 nm of gold using an electron-beam evaporator (Angstrom engineering). The substrates were then sonicated in anhydrous ethanol to remove the spheres, leaving a hexagonal array of gold nanoprisms [16].

Single Beam Induced Surface Gratings and Diazonium Salt Grafting: To inscribe the grating structures on the bare glass, the substrates were positioned over an inverted microscope equipped with a 632.8 nm laser. A 5 mM solution of 4-nitrobenzenediazonium tetrafluoroborate was prepared in MilliQ water (18.2 Ω) and drop-cast onto the surface of the substrates. A rubber O-ring was used to keep the solution on top of the structures during irradiation and to prevent the samples from drying. Irradiation was performed through a 20× objective (N.A. = 0.5) with a laser intensity of 5.9 mW for a varying length of time. The sample stage was lowered past the focal point to generate a wider beam spot. After irradiation, the samples were washed with MilliQ water and dried under a gentle flow of nitrogen gas. A similar procedure was performed to graft the diazonium salts on the plasmonic substrates.

Finite-Difference Time-Domain (FDTD) simulations: The electromagnetic modelling was performed using FDTD Solutions (Lumerical). The properties of the simulated structures were set

using the standard titanium and gold material indices on a silicon dioxide substrate [17]. The nanoprisms organized in a hexagonal array were set up using thicknesses of 3 nm for titanium and 30 nm for gold. Simulations with a polarization angle of 90° were performed in a similar manner by rotating the input polarization of the light source while maintaining the proper boundary conditions. The amplitude of the input planar wave field was set to 1 V/m for the simulations. A total-field scattered-field light source with a wavelength range of 400 to 1000 nm was employed. The electromagnetic enhancement maps were calculated at the surface of the nanostructure at a wavelength of 630 nm during the simulation.

Scanning Electron Microscopy (SEM): Scanning electron microscopy was performed using a LEO 1530 field emission SEM (Zeiss). Samples on non-conductive substrates (i.e., bare glass) were coated with ~5 nm of osmium prior to imaging to prevent charging on the surface.

Atomic Force Microscopy (AFM): AFM scans were obtained using a BioScope Catalyst atomic force microscope (Bruker). Silicon tips (NCL-50, NanoWorld) with a force constant of 48 N/m and a resonance frequency of 190 kHz were used in tapping mode. Height images were recorded at a scan rate of 0.3 Hz to acquire sample topography. Image processing and extraction of cross-sections were performed using Gwyddion software.

3. Results and Discussion

The irradiation of the diazonium salt solution on a bare glass substrate results in the formation of ripples parallel to the direction of the polarization. The cationic reaction of the diazonium salt in solution, which is commonly referred to as spontaneous grafting, will result in aggregates of a polyaryl film. These aggregates can then adhere to the glass surface. In this process, which can be induced by heat or light, the heterolytic dediazonation of the salt forms cations that react with one another, resulting in the formation of the initial polyaryl thin film (Fig. 1a) [18-20]. The SEM

image of the polyaryl thin film (Fig. 1a) was treated with color segmentation using Python for a higher contrast to highlight the difference between the polyaryl thin film (blue) and the bare glass (white).

The self-organized grating formation begins when the incident beam is scattered around nanoscale surface irregularities of the polyaryl thin film. The incident beam scattering causes a ripple-like interference pattern across the surface with high and low intensity areas [14, 21]. A longer irradiation time results in the enhanced formation of the periodic structures (Fig. 1b). A similar process initiates the grating formation on the plasmonic substrates. The hot spots generated by the plasmonic nanostructures act as nucleation sites for the grating formation. The nucleation sites affect both the pitch and the pattern of the grating.

The grating pitch can be determined using the phase matching condition (Eq. 1). When an electromagnetic wave is incident on an interface, Maxwell equations' boundary condition requires that the tangential component of the light be continuous (Fig. 1b). The longitudinal vector component can then be derived using the dispersion relation (Eq. 2).

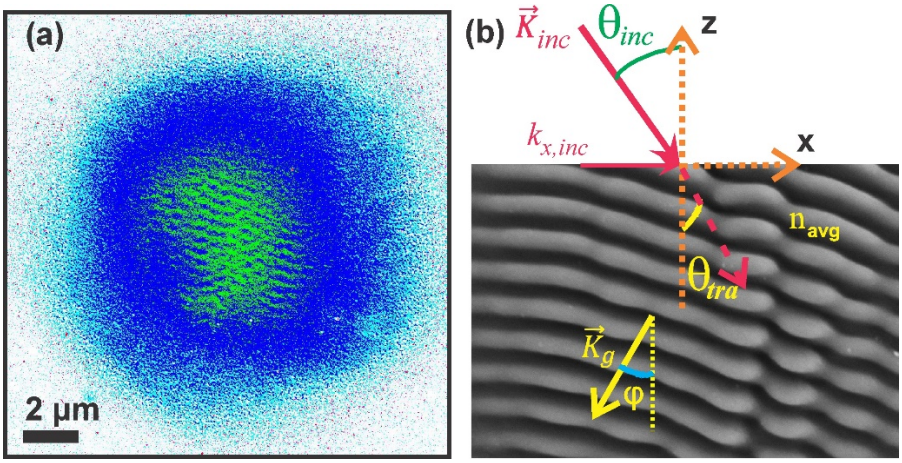

Fig. 1. a) A high contrast SEM image of the polyaryl thin film formation on glass substrate after 2 minutes of irradiation (original provided as Fig. S1). b) Schematic illustration of the grating k-vector and the light k-vector. The grating is fully formed after 8 minutes of irradiation.

Phase-matching condition:

$$\vec{k}_{tra,x} = \vec{k}_{inc,x} \pm m\vec{k}_{g,x} \qquad \text{(Eq. 1)}$$

Dispersion relation:

$$|\vec{k}_{tra,z}|^2 = |n_{avg}\vec{k}_{inc}|^2 - |\vec{k}_{tra,x}|^2 \qquad \text{(Eq. 2)}$$

Where n_{avg} is the refractive index just above the material interface, m is the diffraction order, $\mathbf{k}_{inc}$ is the incident light wavevector, $\mathbf{k}_{tra}$ is the light wavevector in the transmission region, and $\mathbf{k}_g$ is the grating wavevector. Considering Eqs 1-2, the grating periodicity Λ becomes (Eq. 3):

$$\Lambda = \frac{\pm m\lambda_{inc} \sin\varphi}{(n_{avg} \sin\theta_m - n_{inc} \sin\theta_{inc})} \qquad \text{(Eq. 3)}$$

Where θ_m is the diffraction angle, θ_{inc} is the incident angle, φ is the angle between the normal to plane and the grating vector, and λ_{inc} is the wavelength of incident radiation. For a grating with crests and troughs running perpendicular to electric field (grating vector parallel to the electric field $\varphi = 90^o$), the diffraction at grazing angle $\theta_m = 90^o$ and normal irradiation $\theta_{inc} = 0^o$, the equation can be simplified to:

$$\Lambda = \frac{\lambda}{n_{avg}} \qquad \text{(Eq. 4)}$$

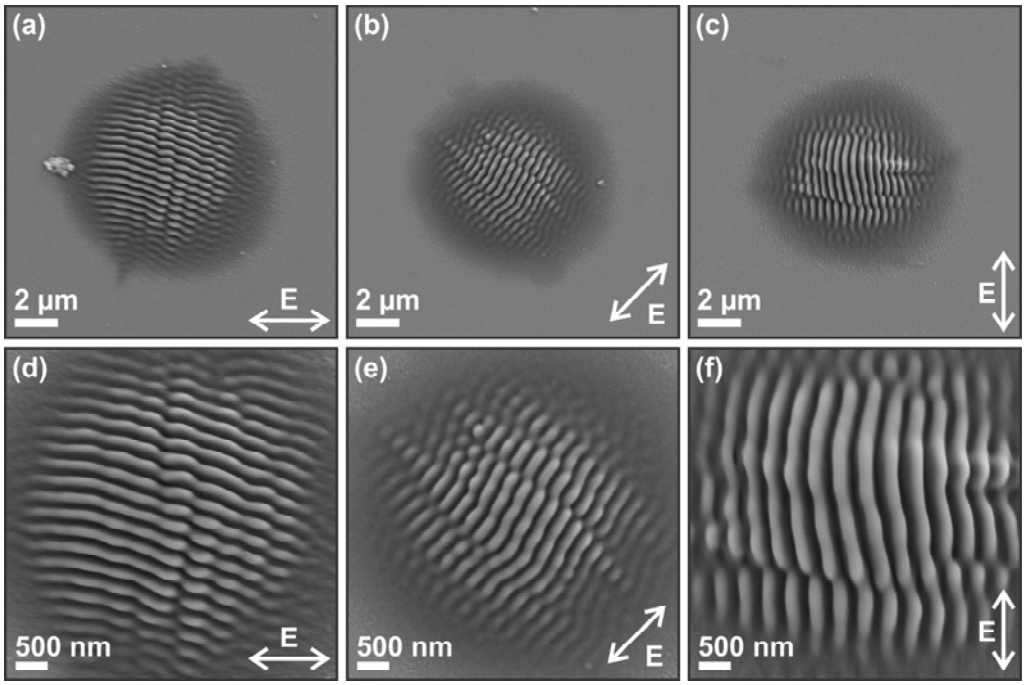

Fig. 2. (a-c) SEM images of the gratings produced on glass with a polarization of 0°, 45°, and 90°, respectively. (d-f) Higher magnification images of (a-c), respectively. Patterns were obtained after an irradiance of 7.49×10^3 W/cm^2 for 8 minutes.

Three gratings were inscribed onto a bare glass substrate after 8 minutes of irradiation with distinct polarization orientations of the single beam (Fig. 2). When the input polarization is rotated, the resulting grating orients accordingly. The formation of these gratings is dependent on incident intensity. The 20× microscope objective (N.A. = 0.5) was slightly defocused to increase the beam size at the sample plane. The resulting size of the laser beam was approximately 10 μm. For this defocused beam, the average irradiance across the surface is 7.49×10^3 W/cm^2, much lower than the irradiance corresponding to the focused beam spot (7.49×10^5 W/cm^2). The lower irradiance allowed by the defocused beam results in the formation of periodic ripple structures. In contrast, with a focused beam, the ripples form only around the edges of the laser spot with an irregular structure in the center (Fig. S2). Under high irradiance, there is not enough time for the self-

organization process. Instead, material deformation occurs over the entire irradiated area, forming irregular structures. Under low irradiance, this surface deformation does not occur. The grating amplitude increases with increasing irradiation time. After 10 minutes of irradiation, more material accumulates, and the ripple structures begin to recombine due to lack of space. Using AFM, we determined that the overall structure heights produced during the 8-minute irradiation were approximately 1.1 μm (Fig. 3a-b) at its maximum and the periodicity at the center of the grating of 390±20 nm. Due to the gaussian nature of the laser, the grating structures produced further exhibit a gaussian profile (Fig. 3b).

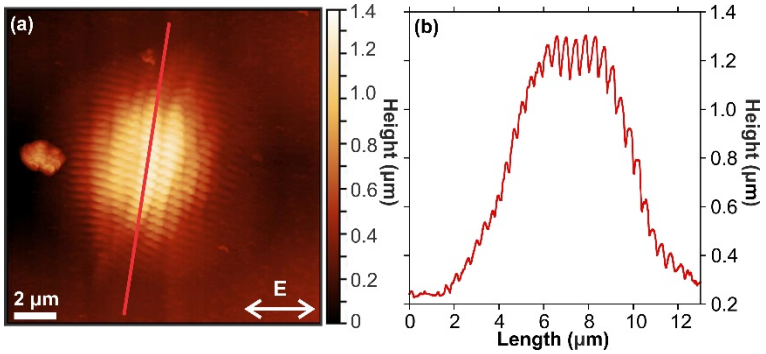

Fig. 3. (a) AFM scan of the grating produced with a polarization of 0° (same structure as shown in Fig 1a). (b) Cross section of (a) as indicated in red.

To ascertain the absence of interference from reflection within the glass, the pitch of the LIPSS was measured on three glass substrates with thicknesses of 130, 600, and 1000 μm (Fig. S3). The pitch of the grating on all three substrates were measured to be approximately 375 ± 10 nm. Therefore, we can conclude that the substrate thickness does not influence grating formation. Using Eq. 4, we can theoretically determine that a normal incident beam at the interface of the solution and substrate creates gratings with a pitch of 420 nm, where n_{avg} is 1.5. This differs from the experimental result by 10 %. This error can be explained by the fact the grating equation does not consider material response to the incident beam. Although the refractive index at the interface

of the substrate is considered in the equation, the equation does not consider structure growth, which depend on the chemical and physical properties of the material. The intensity dependence of chemical reduction of the diazonium salt are key factors in the structure growth.

Plasmonic gold nanoprisms organized in a hexagonal geometry were produced using NSL to investigate directional control of the reduction of diazonium salts into a polyaryl layer. The plasmon resonance of the NSL substrates was determined to be approximately 640 nm (Fig. 4a), matching the excitation wavelength of the laser (632.8 nm). This allows for the excitation of the localized surface plasmon resonance on the nanoprism surfaces. Plasmon resonances can be used to induce chemical reactions through several reaction pathways, including thermal and hot-carrier processes [22-23]. In plasmon-mediated chemical reactions on nanostructures, grafting is dominated by a radical reaction since thermal effects dissipate very quickly in the solution [24]. In the radical reaction, hot electrons generated by light excitation are transferred from the gold structures to the diazonium cation, resulting in the formation of aryl radicals. These radicals react with the surface to form an aryl layer which continues to grow into a thin polymer film. The thickness of this polymer film varies with the irradiation conditions and local field enhancements. The formation of the polymer thin film is more efficient in the area where the field is maximum. This plasmon-mediated chemistry also eliminates the need for a catalyst to be present, indicating that the reactions are plasmon-induced [16, 25]. In Fig. 4b, we show the plasmon-induced functionalization in the vicinity of gold nanoprisms upon irradiation at 632.8 nm.

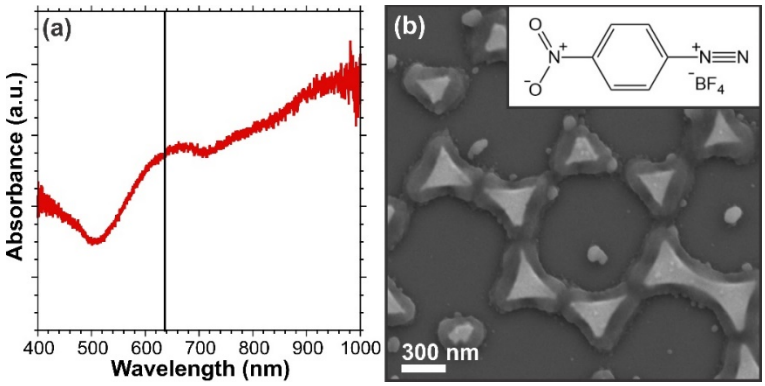

Fig. 4. (a) Absorbance measurements of the NSL substrates with the 632.8 nm irradiation wavelength indicated by the black line. (b) An SEM image of the inset molecule grafted to the surface using a 632.8 nm laser after 3 minutes of irradiation with an irradiance of 7.49×10^3 W/cm^2.

The diazonium salt appears to form a polyaryl layer coating around the individual gold nanostructures. Noticeably, when two triangles are facing each other, the small gap between the triangle where the field is the most concentrated further enhance the photoinduced grafting with larger amounts of grafted material.

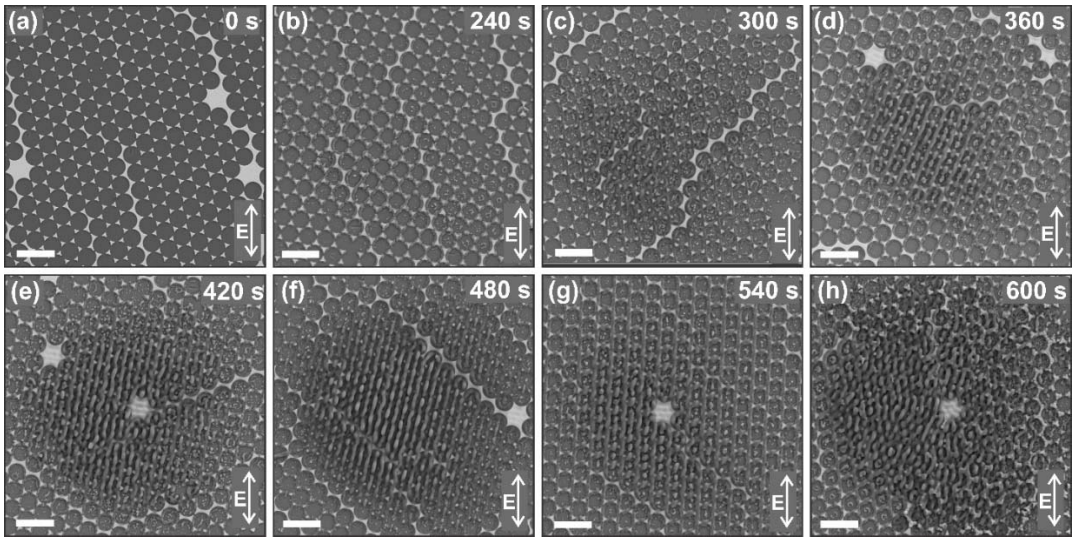

Fig 5. SEM images of the grating produced on an NSL substrate for different irradiation times, as indicated in the top right of each panel. The scale bar is 2 μm.

As the irradiation time of diazonium salt-containing solution on the NSL structures increases, self-organized gratings emerge (Fig. 5). After 4 minutes of irradiation, the diazonium salt grafting to the surface is noticeable (Fig. 5b) compared to the non-irradiated section (Fig. 5a). After 5 minutes of irradiation, an even larger grafting amount is visible (Fig. 5c). A wider grating pitch of roughly 455 ± 10 nm compared to 375 nm on a glass substrate is observed after 6 minutes of irradiation (Fig. 5d). While the gratings along the edges of the nanoprisms form more quickly, the ridges between the structures take longer to form. This is highlighted in Fig. 5d, where prominent grating line alternates with a line of smaller amplitude. For longer irradiation times, the grating produced becomes more uniform (Fig. 5f, g). The accumulation of material away from the nanoprisms after 10 minutes of irradiation seems to influence the structure pattern resulting in a loss of order (Fig. 5h).

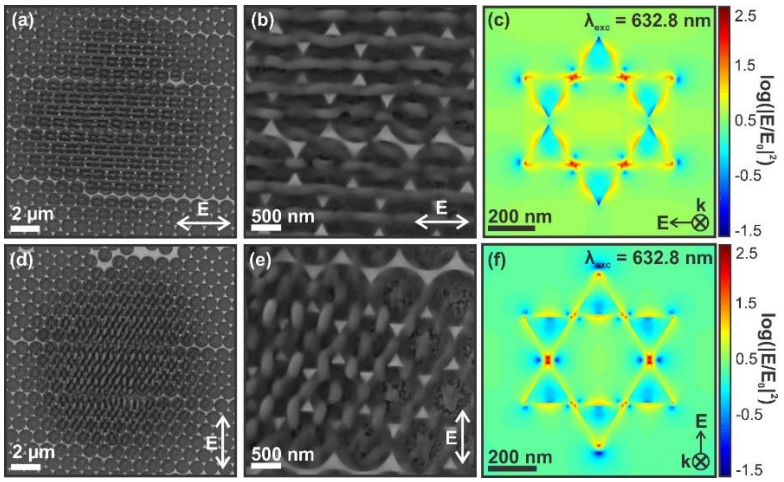

Fig. 6. SEM images and FDTD calculations for grafting on an NSL substrate for horizontal (a-c) and vertical (d-f) polarizations.

The spatial distribution of the electromagnetic enhancement was investigated using FDTD modelling to follow the grating growth and evaluate the polarization dependence (Fig. 6c, f). Gratings were inscribed using horizontal (Fig. 6a-c) and vertical polarizations (Fig. 6d-f). When

the polarization of the excitation source is along the base of the nanoprisms (Fig. 6c), the coupling between the plasmons at the apices of the adjacent nanoprisms is efficient and forms a series of aligned hotspots. When the input polarization is oriented along the height of the nanoprisms, two main hot spots can be observed at the junction between nanoprisms (Fig. 6f), and the center of the hexagonal lattice does not show any significant enhancement. In both cases, an enhancement of the electric field is observed, and a significantly higher enhancement factor is present at the apices of the triangles. These plasmon resonances can be used as guides to effectively direct plasmon-mediated chemical reactions in the vicinity of the metallic nanotriangles, and to even modify the pitch of the self-organized ripples.

When the polarization is aligned with the bases of the triangles (Fig. 6a, b), the ripple structures are fully formed with a wider pitch as compared with bare substrate due to the alignment of the structures with the direction of plasmon-guided reactions. The electric field enhancement from the nanoprisms directs the pitch of the gratings. When the electric field enhancement is aligned along the base of the triangles, the nanoprisms perturbate the nucleation of the gratings by acting as a barrier and disturb the initial process of the interference pattern formation. However, when the polarization is aligned along the height of a triangle, a crisscross pattern is observed (Fig. 6d, e). The coupling between the plasmon resonances of the nanoprism apices acts as a physical guide to the reduction of the diazonium salts to the substrate surface. In a polarization configuration perpendicular to the triangle bases, the nucleation for the grating deviates from straight lines to a crisscross pattern. At the center of the lattices, the self-organization process follows the polarization direction in a similar fashion as on bare glass substrate. At the junction between nanoprisms, the hotspot generations perturbate the self-organization process and induce a different direction for grating formation.

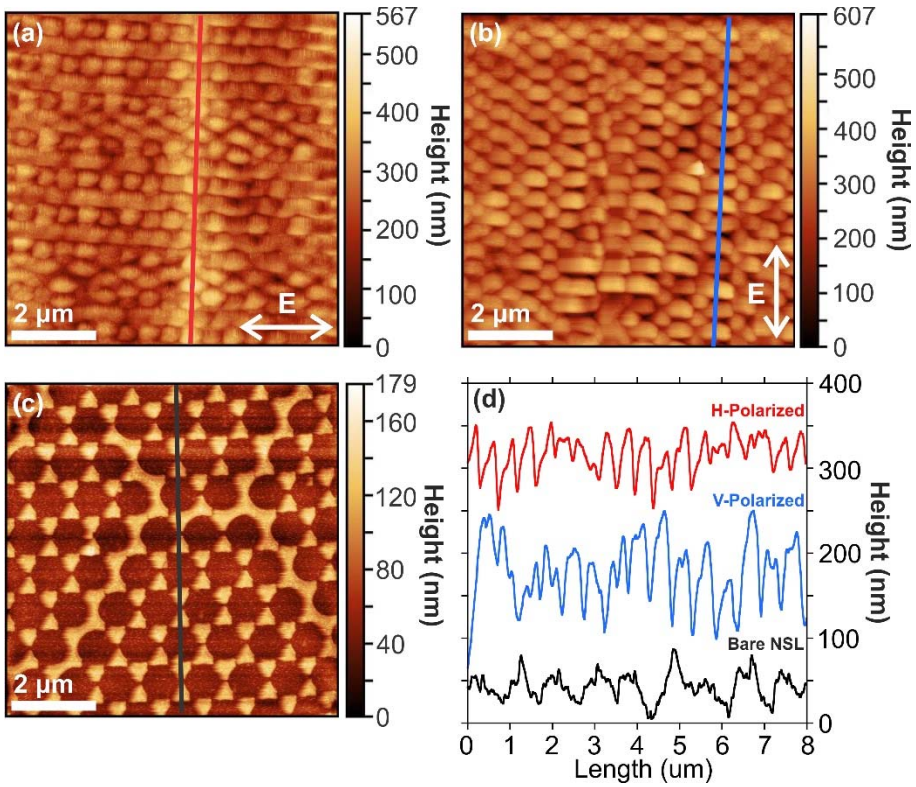

Fig. 7. AFM scans of the grafting produced on the NSL substrates using (a) a horizontally polarized laser and (b) a vertically polarized laser, as well as (c) the bare NSL substrate. (d) The cross sections for (a), (b), and (c) are shown in red, blue, and black, respectively. The cross sections have been shifted in the y-axis for clarity.

The height profiles of the gratings produced on the NSL were obtained using AFM (Fig. 7d). The grafting on both the horizontally- (Fig. 7a) and vertically-polarized (Fig. 7b) irradiated substrates show a height roughly 100 nm higher than the bare nanoprisms (Fig. 7c). This indicates that the accumulated material that comprises the polyaryl film is roughly 100 nm in height. Furthermore, the gratings produced with both polarizations no longer show a Gaussian profile. This further indicates that the nanoprisms actively direct the grafting occurring at the surface.

This simple self-developing and polarization-dependent procedure makes these single beam structures possible candidates for a variety of photonic applications. The process of self-

organization on solids and in liquids can be used for polarization sensitive devices [26]. Furthermore, the sensitivity of the self-organized gratings on plasmonic substrates make them interesting candidates for plasmonic sensors [16, 27]. The self-organized grafting of the diazonium salt on the nanoprisms demonstrates the effectiveness of plasmon-mediated chemistry to trigger spatially controlled and polarization-dependent surface reactions [28-30]. This process can potentially be used to graft molecules with distinct chemical functions into periodic gratings over nanostructures at specific wavelengths.

4. Conclusion

Herein, we reportgrafting and self-organized grating formation triggered by plasmon-mediated reduction of a diazonium salt. Irradiation of the diazonium salt solution on NSL structures initially results in homogenous grafting around the nanoprisms. Longer irradiation times facilitate the self-organization of periodic ripples. The ripple structures on a bare glass substrate follow a self-organization process. The pitch of the ripples follows the grating equation derived with the incident laser wavelength and the refractive index of the diazonium salt solution at the interface with the glass. In the presence of metallic nanostructures, localized field enhancement at the apices of the triangles disturb the initial growth of the self-organized interference pattern, resulting in the chemical reduction of diazonium salts into polyaryl layers. When the polarization is aligned with the triangle bases ripples form with a larger periodicity compared to those on the glass substrates. When the polarization is aligned perpendicular to the triangle bases, a crisscross pattern is instead formed. More complex metallic structures could be fabricated by more sophisticated nanolithographic techniques such as electron beam lithography to further investigate plasmon-mediated patterning. Additionally, other wavelengths and distinct polarization states can be

explored, opening the possibility of multiplexing polymers onto nanostructures using light with moderate intensity.

Credit author statement

Denis A.B. Therien is the first author of the work and collected most of the experimental data.

Nina M. Ćulum performed AFM scans and image processing.

Danielle M. McRae helped with FDTD simulations.

Leila Mazaheri assisted with conceptualization and research methods.

François Lagugné-Labarthet assisted with conceptualization of the entire manuscript.

All authors have given approval of the final version of the manuscript.

Declaration of competing interest

The authors declare that they have no know competing financial interests or personal relationships that could have appeared to influence the work reported in this paper.

Acknowledgments

The authors would like to gratefully acknowledge the Nanofabrication Facility at Western University for their assistance with SEM imaging. This research was supported by the Natural Sciences and Engineering Research Council (NSERC) of Canada through a Strategic Partnership grant (STP 521543-18).

References

[1]. A. Siegman, P. Fauchet, Stimulated Wood's anomalies on laser-illuminated surfaces, IEEE J. Quantum Electron. 22 (1986) 1384-1403.
[2]. J. Bonse, J. Krüger, S. Höhm, A. Rosenfeld, Femtosecond laser-induced periodic surface structures, J. Laser Appl. 24 (2012) 042006.
[3]. J. Bonse, S. Höhm, S. V. Kirner, A. Rosenfeld, J. Krüger, Laser-induced periodic surface structures—A scientific evergreen, IEEE J. Sel. Top. Quantum Electron. 23 (2017) 9000615.
[4]. L. Hong, Rusli, X. C. Wang, H. Y. Zheng, H. Wang, H. Y. Yu, Femtosecond laser fabrication of large-area periodic surface ripple structure on Si substrate, Appl. Surf. Sci. 297 (2014) 134-138.
[5]. H. Zhang, J.-P. Colombier, S. Witte, Laser-induced periodic surface structures: Arbitrary angles of incidence and polarization states, Phys. Rev. B 101 (2020) 245430.
[6]. J. Sipe, J. F. Young, J. Preston, H. Van Driel, Laser-induced periodic surface structure. I. Theory, Phys. Rev. B 27 (1983) 1141.
[7]. J. Elson, K. Ritchie, Diffuse scattering and surface-plasmon generation by photons at a rough dielectric surface, Phys. Status Solidi B 62 (1974) 461-468.
[8]. A. Rudenko, C. Mauclair, F. Garrelie, R. Stoian, J.-P. Colombier, Self-organization of surfaces on the nanoscale by topography-mediated selection of quasi-cylindrical and plasmonic waves, Nanophotonics 8 (2019) 459-465.
[9]. Y. Fuentes-Edfuf, J. A. Sánchez-Gil, C. Florian, V. Giannini, J. Solis, J. Siegel, Surface plasmon polaritons on rough metal surfaces: Role in the formation of laser-induced periodic surface structures, ACS Omega 4 (2019) 6939-6946.
[10]. X. He, A. Datta, W. Nam, L. M. Traverso, X. Xu, Sub-diffraction limited writing based on laser induced periodic surface structures (LIPSS), Sci. Rep. 6 (2016) 35035.
[11]. R. Buividas, M. Mikutis, S. Juodkazis, Surface and bulk structuring of materials by ripples with long and short laser pulses: Recent advances, Prog. Quantum. Electron. 38 (2014) 119-156.
[12]. L. Mazaheri, R. G. Sabat, O. Lebel, J.-M. Nunzi, Unraveling the nucleation and growth of spontaneous surface relief gratings, Opt. Mater. 62 (2016) 378-391.
[13]. H. Leblond, R. Barille, S. Ahmadi-Kandjani, J.-M. Nunzi, E. Ortyl, S. Kucharski, Spontaneous formation of optically induced surface relief gratings, J. Phys. B Atom Mol. Opt. Phys. 42 (2009) 205401.
[14]. J. Bonse, S. Gräf, Maxwell meets Marangoni—A review of theories on Laser-Induced Periodic Surface Structures, Laser Photonics Rev. 14 (2020) 2000215.
[15]. I. Tijunelyte, I. Kherbouche, S. Gam-Derouich, M. Nguyen, N. Lidgi-Guigi, M. Lamy de la Chapelle, A. Lamouri, G. Lévi, J. Aubard, A. Chevillot-Biraud, C. Mangeney, N. Félidj, Multi-funtionalization of lithography designed gold nanodisks by plasmon-mediated reduction of aryl diazonium salts, Nanoscale Horiz. 3 (2018) 53-57.
[16]. V.-Q. Nguyen, Y. Ai, P. Martin, J.-C. Lacroix, Plasmon-induced nanolocalized reduction of diazonium salts, ACS Omega 2 (2017) 1947-1955.
[17]. E. D. Palik, Handbook of optical constants of solids, Academic Press, Burlington, 1997.
[18]. J. Pinson, F. Podvorica, Attachment of organic layers to conductive or semiconductive surfaces by reduction of diazonium salts, Chem. Soc. Rev. 34 (2005) 429-439.
[19]. A. Mesnage, X. Lefèvre, P. Jégou, G. Deniau, S. Palacin, Spontaneous grafting of diazonium salts: chemical mechanism on metallic surfaces, Langmuir 28 (2012) 11767-11778.

[20]. D. R. Jayasundara, R. J. Cullen, P. E. Colavita, In situ and real time characterization of spontaneous grafting of aryldiazonium salts at carbon surfaces, Chem. Mater. 25 (2013) 1144-1152.
[21]. A. Rudenko, J.-P. Colombier, S. Höhm, A. Rosenfeld, J. Krüger, J. Bonse, T. E. Itina, Spontaneous periodic ordering on the surface and in the bulk of dielectrics irradiated by ultrafast laser: a shared electromagnetic origin, Sci. Rep. 7 (2017) 1-14.
[22]. G. Baffou, I. Bordacchini, A. Baldi, R. Quidant, Simple experimental procedures to distinguish photothermal from hot-carrier processes in plasmonics, Light Sci. Appl. 9 (2020) 108.
[23]. A. Mesnage, X. Lefèvre, P. Jégou, G. Deniau, S. Palacin, Spontaneous grafting of diazonium salts: chemical mechanism on metallic surfaces, Langmuir 28 (2012) 11767-11778.
[24]. O. Guselnikova, P. Postnikov, M. M. Chehimi, Y. Kalachyovaa, V. Svorcik, O. Lyutakov, Surface plasmon-polariton: a novel way to initiate azide–alkyne cycloaddition, Langmuir 35 (2019) 2023-2032.
[25]. M. Busson, A. Berisha, C. Combellas, F. Kanoufi, J. Pinson, Photochemical grafting of diazonium salts on metals, Chem. Commun. 47 (2011) 12631-12633.
[26]. R. Chen, Y. H. Lee, T. Zhan, K. Yin, Z. An, S. T. Wu, Multistimuli-responsive self-organized liquid crystal Bragg gratings, Adv. Opt. Mater. 7 (2019) 1900101.
[27]. S. Nair, C. Escobedo, R. G. Sabat, Crossed surface relief gratings as nanoplasmonic biosensors, ACS Sensors 2 (2017) 379-385.
[28]. M. Nguyen, I. Tijunelyte, M. L. de la Chapelle, C. Mangeney, N. Félidj, Plasmon-driven surface functionalization of gold nanoparticles, In: Plasmonics in Chemistry and Biology, 1st ed.; de la Chapelle, M. L.; N. Félidj, Eds. Jenny Stanford Publishing: New York, (2019) 1-32.
[29]. I. Kherbouche, Y. Luo, N. Félidj, C. Mangeney, Plasmon-mediated surface functionalization: new horizons for the control of surface chemistry at the nanoscale, Chem. Mater. 32 (2020) 5442–5454.
[30]. Y. Luo, Y. Xiao, D. Onidas, L. Iannazzo, M. Etheve-Quelquejeu, A. Lamouri, N. Félidj, S. Mahouche, T. Brulé, N. Eilstein, F. Gazeau, C. Mangeney, Raman reporters derived from aryl diazonium salts for SERS encoded-nanoparticles, Chem. Commun. 56 (2020) 6822-6825.